Journal of ELECTRONIC MATERIALS, Vol. 46, No. 8, 2017
DOI: 10.1007/s11664-017-5471-3

Bulk Crystal Growth, and High-Resolution X-ray Diffraction Results of LiZnAs Semiconductor Material

BENJAMIN W. MONTAG,[1,3] MICHAEL A. REICHENBERGER,[1] MADHANA SUNDER,[2] PHILIP B. UGOROWSKI,[1] KYLE A. NELSON,[1] LUKE C. HENSON,[1] and DOUGLAS S. MCGREGOR[1]

1.—Semiconductor Materials and Radiological Technologies (S.M.A.R.T) Laboratory, Kansas State University, Manhattan, KS 66506, USA. 2.—Bruker AXS Inc, 5465 E. Cheryl Parkway, Madison, WI 53711, USA. 3.—e-mail: bmontag@ksu.edu

LiZnAs is being explored as a candidate for solid-state neutron detectors. The compact form, solid-state device would have greater efficiency than present day gas-filled ^{3}He and $^{10}BF_3$ detectors. Devices fabricated from LiZnAs having either natural Li (nominally 7.5% ^{6}Li) or enriched ^{6}Li (usually 95% ^{6}Li) as constituent atoms may provide a material for compact high efficiency neutron detectors. The $^{6}Li(n,t)^{4}He$ reaction yields a total Q-value of 4.78 MeV, an energy larger than that of the ^{10}B reaction, which can easily be identified above background radiations. LiZnAs material was synthesized by preparing equimolar portions of Li, Zn, and As sealed under vacuum (10^{-6} Torr) in quartz ampoules lined with boron nitride and subsequently reacted in a compounding furnace (Montag et al. in J Cryst Growth 412:103, 2015). The raw synthesized LiZnAs was purified by a static vacuum sublimation in quartz (Montag et al. in J Cryst Growth 438:99, 2016). Bulk crystalline LiZnAs ingots were grown from the purified material with a high-temperature Bridgman-style growth process described here. One of the largest LiZnAs ingots harvested was 9.6 mm in diameter and 4.2 mm in length. Samples were harvested from the ingot and were characterized for crystallinity using a Bruker AXS Inc. D8 AXS Inc. D2 CRYSO, energy dispersive x-ray diffractometer, and a Bruker AXS Inc. D8 DISCOVER, high-resolution x-ray diffractometer equipped with molybdenum radiation, Gobel mirror, four bounce germanium monochromator and a scintillation detector. The primary beam divergence was determined to be 0.004°, using a single crystal Si standard. The x-ray based characterization revealed that the samples nucleated in the (110) direction and a high-resolution open detector rocking curve recorded on the (220) LiZnAs yielded a full width at half maximum (FWHM) of 0.235°. Sectional pole figures using off-axis reflections of the (211) LiZnAs confirmed in-plane ordering, and also indicated the presence of multiple domains. The LiZnAs bulk crystals exhibited a Primitive Cubic Bravais lattice instead of the commonly reported Face-centered Cubic Bravais lattice. The lattice constant was determined to be 5.5146 ± 0.0003 Å.

Key words: Lithium compounds, radiation, semiconducting ternary compounds, x-ray diffraction, crystal structure, bridgman technique

INTRODUCTION

Nowotny–Juza materials were studied as early as the 1960s. The ternary compounds were originally

(Received June 27, 2016; accepted March 21, 2017; published online April 6, 2017)

studied, and are still used today for photonic applications.[3–5] The filled tetrahedral compound class $A^{I}B^{II}C^{V}$ materials consist of the III–V-like compounds with the group I element, lithium, located at the interstitial site. Unlike thin-film and doped devices, the concentration of Li atoms is equal to other constituent atoms. These materials are also inherently desirable for their zincblende cubic crystal structure, which is typically arranged with a F-43m space group. The group II atom is located at $\tau_1 = (0, 0, 0)a$ where a is the lattice constant, and the group V atom is located at $\tau_2 = (1/4, 1/4, 1/4)a$. Lithium atoms, group I, fill the interstitial site at $\tau_3 = (1/2, 1/2, 1/2)a$, resulting in a lithium-loaded semiconducting material. In the following study, however, bulk grown LiZnAs samples were determined to possess a Primitive Cubic Bravais lattice with a basis of several atoms.

Ternary compounds, LiZnAs and LiZnP, have been synthesized in the past, commonly in a graphite lined crucible within a quartz ampoule.[6] LiZnP has been synthesized in a tantalum lined crucible contained in vacuum sealed quartz ampoules as described by Kuriyama[7] However, bulk growth of these materials has not been reported. In the existing literature, material and electrical properties have been reported from samples procured by direct reaction of elemental and/or binary materials.[3–7] Unfortunately, these samples are generally tiny facets extracted from the reaction mixture, and are usually small and extremely difficult to handle and process into devices.

Numerous materials containing ^{6}Li, ^{10}B, ^{113}Cd, ^{157}Gd and ^{199}Hg have been considered for solid-state neutron detectors.[8–19] ^{10}B has a microscopic thermal neutron absorption cross-section of 3839 barns. However, boron-based compounds, such as BP, BN, and BAs have shown limited success, and work is still being performed to resolve crystal growth and materials preparation problems.[16–19] Thin-film boron devices have been explored and have appeared promising; however, they suffer in performance due to their geometry, where only one reaction product can be absorbed in a semiconducting material, therefore producing some signals that can be difficult to distinguish from background and gamma-ray induced events.[20] Additionally, the reactive film thickness is limited because of the reaction product self-absorption, and, therefore, thermal neutron absorption is limited, consequently resulting in a maximum intrinsic detection efficiency of approximately 4.5%.[20] Solid-state materials containing ^{113}Cd and ^{199}Hg devices have also been explored, and have limited detection efficiency due to the low absorption probability of the prompt gamma-rays that result from the ^{113}Cd$(n,\gamma)^{114}$Cd and ^{199}Hg$(n,\gamma)^{200}$Hg reactions.[8–11] The ^{157}Gd$(n,\gamma)^{158}$Gd reaction is interesting for the large ^{157}Gd thermal neutron capture cross-section of 240,000 barns, however unfortunately, the ^{157}Gd$(n,\gamma)^{158}$Gd reaction yields a spectrum of low energy prompt gamma rays and, low energy conversion electrons, all of which are difficult to discern from background radiations.[20] Finally, ^{6}Li has not been explored as extensively as other thermal neutron absorbers, and has an intrinsic thermal neutron absorption cross-section of 940 barns. The reaction produces a total Q-value of 4.78 MeV, described by the following reaction,

$$^{6}\mathrm{Li} + {}^{1}_{0}n \rightarrow {}^{3}\mathrm{H}\ (2.73\ \mathrm{MeV}) + \alpha(2.05\ \mathrm{MeV}). \qquad (1)$$

LiZnAs has been reported to have a bandgap of 1.51 eV at 300 K, an energy gap ideal for a room-temperature semiconductor device.[21] A Hall mobility was reported by Kuriyama at ≤30 cm^2/V s.[22] As a result, some of these reported electrical properties make LiZnAs and other lithium ternary compound materials desirable for compact, high neutron sensitivity, solid-state detectors. However, lithium is very reactive, and the high pressures that are developed due to the exothermic reactions that occur during the reaction process often results in containment failure. It was determined that preparing the alloy, Li-Zn, prior to reaction aided the reaction process, and resulted in a much higher ampoule yield.[1] The difficulties in the synthesis and handling processes limit the available physical and electrical property data[3,4,6,21–26] and needs to be further explored. The following study is a contribution to the existing material property data; a procedure to grow bulk crystalline LiZnAs material, and a study of the crystallinity.

EXPERIMENTAL PROCEDURES

Described in the following work is a contribution to the existing body of knowledge for bulk LiZnAs materials where a method to grow bulk crystalline LiZnAs material is demonstrated. In addition, methods to characterize the crystalline orientation, degree of crystallinity, and crystalline ordering in these challenging air sensitive materials are demonstrated in detail.

Bulk Crystal Growth

LiZnAs was synthesized, as described elsewhere, in small batches up to 6.0 g.[1] The synthesized material was purified by a static sublimation process, which successfully separated the ternary LiZnAs material from elemental and binary residual materials that often resulted from the synthesis process.[2] The purified LiZnAs material was subsequently grown into bulk crystals under a high-temperature vertical Bridgman technique described in the following.

Crystal growth in conventional quartz ampoules failed due to the high temperatures necessary to melt LiZnAs. As a result, LiZnAs ingots were grown from melt while contained in welded tantalum ampoules using a low voltage/high current power source (Fig. 1). The process for ampoule and crystal growth preparation is described in detail elsewhere.[27] The

current was ramped on the low voltage/high current power source from 0 amps to approximately 290–305 amps over the course of at least an hour, until an optical thermometer measured approximately 1240°C at the tantalum surface. This unique crystal growth design makes the sample containment, or ampoule (tantalum) the heating element. The technique allows for a high-temperature crystal growth from melt, and does not suffer from the containment problems associated with quartz. Temperature was maintained for at least an hour to ensure a congruent melt. The system was then ramped down to room temperature over a period of 40 hours. In this technique, the heat generated is at the center of the ampoule; therefore, the growth crucible was designed as such to orient the material in a position to begin growth from the bottom of the molten material pool. Thereby, as the vessel is reduced in current (heat), crystal growth was promoted from nucleation at the bottom of molten material and propagated to the top as the vessel is slowly cooled to room temperature, a variation of the Bridgman Technique. The vessel was extracted from the chamber, and opened with a pipe cutter under a pure argon environment. The ingot was harvested, and individual samples were cut from the ingot using a Laser Technology West Ltd. CS400 diamond wire saw for further processing.

X-ray Diffraction Measurements

A LiZnAs sample was diced to 4.155 × 4.060 × 2.100 mm^3, and XRD analysis was performed on one side of the 4.155 × 4.060 mm face. The sample was mounted onto a polishing fixture and was polished in a procedure described elsewhere.[27] An example of a polished sample of purified LiZnAs is shown in Fig. 2. The polished sample was mounted under argon between two Mylar sheets using a custom sample holder designed to keep the sample air-tight.

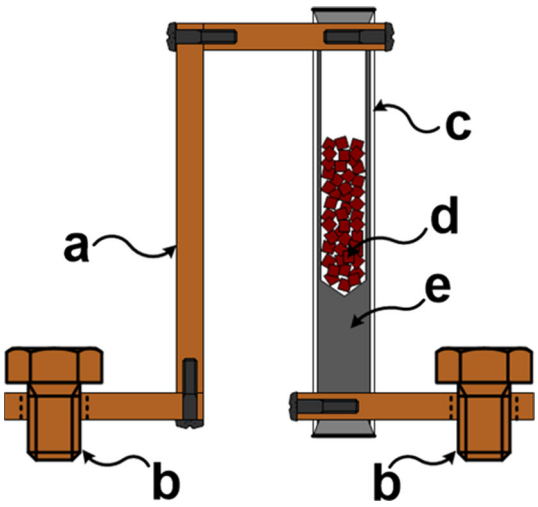

Fig. 1. Cross-section of the tantalum ampoule as loaded into the copper harness for crystal growth. (a) Oxygen-free copper, (b) electrodes, (c) tantalum tube, (d) LiZnAs material, (e) pyrolytic graphite crucible.

Following which, the sample was characterized on a D2 CRYSO energy-dispersive x-ray diffractometer (EDXRD), in order to determine the out-of-plane orientation, degree of miscut and *d* spacing. The sample was then mounted into an air-tight poly (methyl methacrylate) (PMMA) plastic sample holder with a plastic dome using double sided tape, under argon. The sample was then characterized for out-of-plane orientation, mosaic spread and in-plane ordering using a high-resolution D8 DISCOVER x-ray diffractometer.

RESULTS AND CONCLUSIONS

Bulk Crystal Growth

Ingots of various sizes were harvested, the largest being 13.0 mm in length and 9.6 mm in diameter. An ingot grown from purified material was 9.6 mm in diameter and 4.2 mm in length. A sample cut from the purified ingot is shown in Fig. 2. A differential thermal analysis exothermic peak at around 850°C was reported by Kuriyama, and was concluded to be likely a melting, or decomposition, point of LiZnAs.[24] In this study, numerous attempts to grow LiZnAs by melt technique using crucible lined quartz ampoules always resulted in non-congruent melting up to temperatures ≤1150°C, and; therefore, the observation from Kuriyama was not confirmed, nor observed. Temperatures above 1150°C resulted in the expansion of the soft quartz due to the high vapor pressure in the ampoule, and often resulted in ampoule rupture. Bulk crystal growth of LiZnAs requires temperatures slightly above the threshold of conventional resistive coil furnaces that typically have a 1200°C upper limit under continuous operation. Optical thermometer readings sampled through a quartz window of the crystal growth chamber, typically indicated between 1230°C and 1250°C (depending on the focus of the optical thermometer), which allowed for the congruent melt of LiZnAs.

X-ray Diffraction

The polished LiZnAs sample was sandwiched between biaxially-oriented polyethylene terephthalate (BoPET) sheets (Mylar), for protection against moisture and air. The 4.155 × 4.060 mm sample face was evaluated for crystal structure and orientation with a Bruker D2 CRYSO energy-dispersive x-ray diffractometer (EDXRD). The EDXRD method utilizes a rhodium x-ray source that produces a polychromatic x-ray beam, a monocapillary optic to collimate the x-ray beam to a spot and an energy dispersive silicon drift detector. Energy plots of the diffracted beam are collected as the sample is rotated about the crystal surface normal (ϕ). Peaks in the diffracted energy plots correspond to Laue reflections from the crystal. The out-of-plane *d* spacing, degree of miscut and main orientation can be determined from these plots.[28] In the case of the

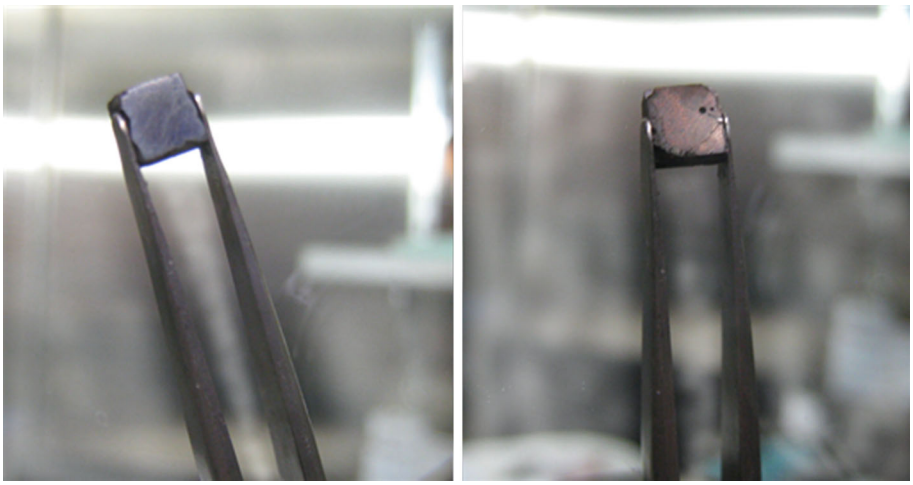

Fig. 2. Both sides of a LiZnAs sample, the sample used for x-ray diffraction analysis. Dimensions: 2.100 × 4.060 × 4.155 mm^3.

LiZnAs sample, Laue peaks are observed for energy values ranging from 2.6 keV to 3.7 keV, 5.3 keV to 7.6 keV, and 8.1 keV to 10.3 keV, as shown in Fig. 3. The mere observation of these peaks is evidence of crystalline ordering in the material being analyzed. The collected spectrum was analyzed using the D2 CRYSO Measure analysis software and a main orientation of (110) was obtained. In addition, an approximate d spacing and lattice constant of the LiZnAs crystal were determined at 1.9 Å and 5.5 Å, respectively. The lattice constant observed, in this case, is different from that of the synthesized material, which had a lattice constant of 5.939 ± 0.002 Å.[1]

Out-of-plane high-resolution XRD measurements were first collected from the 4.155 × 4.060 mm LiZnAs sample face, the same face analyzed by EDXRD. A phase identification scan was collected as shown in Fig. 4. The indexing procedure using the software package, TOPAS (Bruker AXS Inc.), was used to identify the space group.[29] Four peaks were identified each corresponding to the (110), (220), (330) and (440) LiZnAs with a Primitive Cubic Bravais lattice. The Bravais lattice differs from what was seen from synthesized and purified powders[1,2] and what was reported by Bacewicz et al.[6] where a F-43m space group was characterized for LiZnAs powders. Refinement of the phase identification pattern, Fig. 4, using TOPAS yielded a lattice constant of 5.5146 ± 0.0003 Å, which was consistent with what was determined from the EDXRD measurement. The Whole Powder Pattern decomposition approach was used in the refinement procedure.[30] Theoretical phase identification patterns of LiZnAs with a lattice constant of 5.5146 Å for the two different space groups were determined using PowderCell 2.4, and are shown in Figs. 5 and 6 with molybdenum optics of a 0.71 Å wavelength.[31]

Next, the crystalline perfection of the sample was examined by carrying out open detector rocking curves. The 2θ drive was positioned on the (220) reflection (20.931°), and a rocking curve was

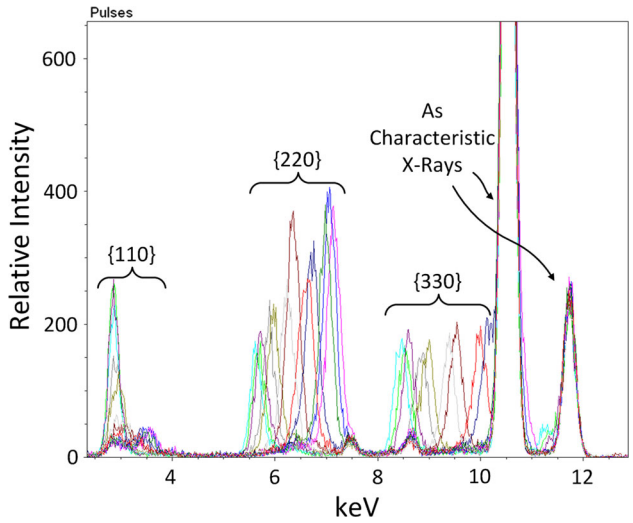

Fig. 3. The EDXRD spectrum for the LiZnAs sample. {110}, {220}, and {330} Laue peaks and characteristic x-ray peaks from arsenic are observed. Peaks in the diffracted energy plots correspond to Laue reflections in the crystal. Each peak within a collection (i.e., {110}, {220} and {330}) corresponds to a single orientation within the family of crystalline planes.

collected, as shown in Fig. 7. The full width at half maximum (FWHM) was determined at 0.235°. In addition, it can be observed that the peak profile is not Gaussian and could indicate the presence of secondary or additional domains in the sample.

The in-plane ordering of the sample was examined by carrying out off-axis phi scans on the (211) LiZnAs reflection. This was performed by tilting the sample in the ψ direction, in angles desirable for in-plane orientations as listed in Table I. Five prominent reflections were observed at 32.6°, 153.0°, 213.2°, 332.8°, and 336.6°, as shown in Fig. 8. Using vector projection math it is evident that the projection of the off-axis (211) LiZnAs on the (110) LiZnAs is along the [1$\bar{1}$2] LiZnAs direction. In other words,

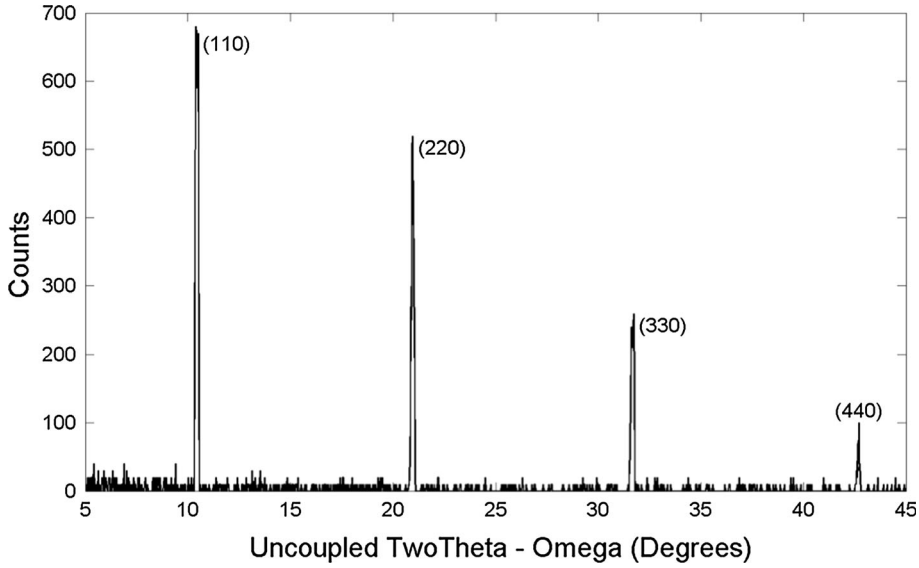

Fig. 4. A phase identification scan of the LiZnAs bulk sample.

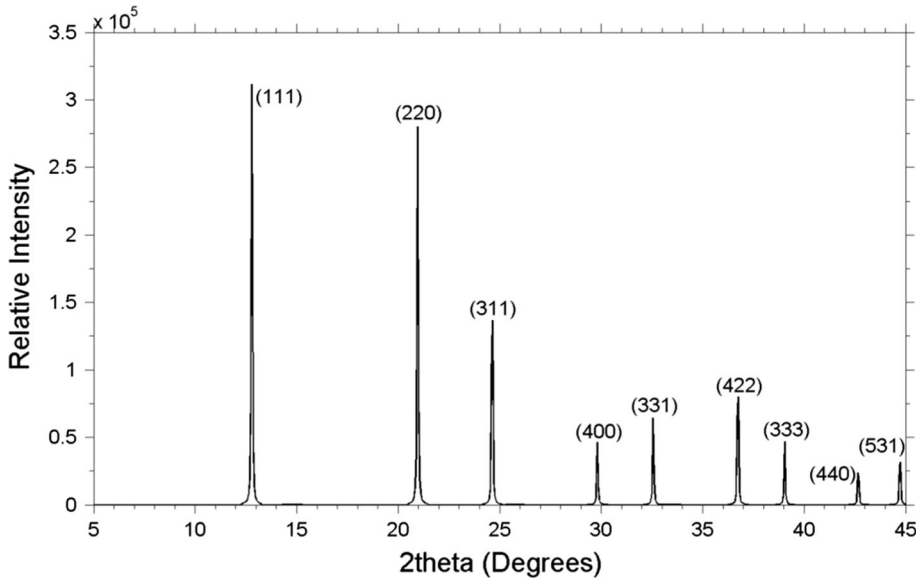

Fig. 5. Theoretical phase identification pattern of a polycrystalline LiZnAs with *F*-43*m* space group, using molybdenum Kα1 radiation. Calculation is performed using PowderCell 2.4.[31]

if the sample were to be a perfect single crystal, four reflections from the {211} LiZnAs family of planes should be observed in the phi scan. In addition, the angular relationship between the {211} LiZnAs planes in the phi scan should match the angular relationship exhibited between the ⟨112⟩ LiZnAs directions projected on the (110) LiZnAs surface, as shown in Fig. 9. However, five reflections were observed in the off-axis (211) LiZnAs phi scan, as shown in Fig. 8, and, in addition, some of the regions of the phi scan exhibited an unusually low background. This is a clear indication that off-axis reflections are coming from multiple domains in the sample. Additionally, some of the (211) LiZnAs reflections are missing from the phi scan due to a high degree of miscut in the polished sample. Complete interpretation of the phi scan results suggests that three major in-plane domains are present in the sample. The in-plane crystallographic relationships in the particular sample that were characterized for one of the domains with respect to the incident x-rays are shown in Fig. 10. An off-axis rocking curve of the (211) orientation was also collected, and resulted in a FWHM of 0.179° as shown in Fig. 11. The rocking curve looks similar to the out-of-plane rocking curve shown in Fig. 7, which is further indication of multiple domains in the sample.

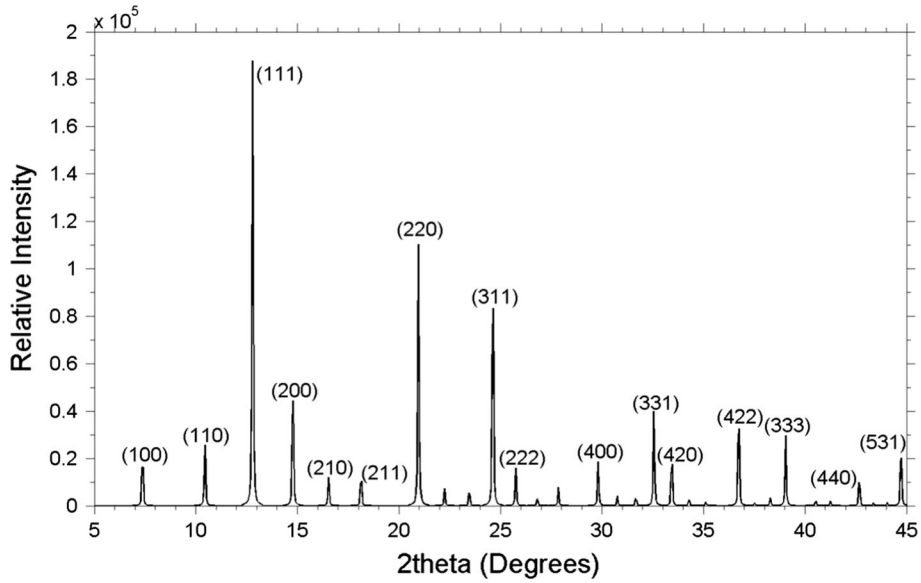

Fig. 6. Theoretical phase identification pattern of a polycrystalline LiZnAs with a primitive space group, using molybdenum Kα1 radiation. Calculation is performed using PowderCell 2.4.[31]

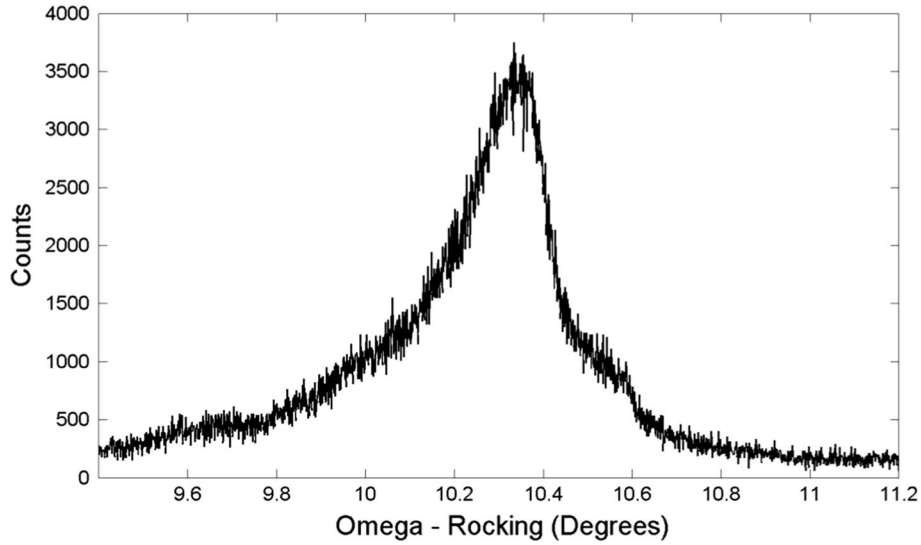

Fig. 7. (220) LiZnAs rocking curve. A full width at half maximum of 0.235° was determined.

DISCUSSION

It is clearly evident that the space group and lattice constant of the bulk LiZnAs crystal is different from the synthesized (5.939 ± 0.002 Å) and purified (5.901 ± 0.002 Å) LiZnAs powders.[1,2] The high-temperature crystal growth method employed for growing bulk crystalline ingots of this material likely led to this change. The LiZnAs crystals grown in this study exhibited a Primitive Cubic Bravais lattice instead of the more commonly observed Face Centered Cubic Bravais lattice. Therefore, these LiZnAs crystals may be lithium deficient with incomplete filling of lithium atoms at interstitial sites. Lithium is very volatile, and the lithium atoms that occupy the interstitial lattice sites, where they may not be bound as tightly in the lattice, can be removed from the interstitial site as a result excessive heat treatment, thereby causing depletion of lithium atoms.[32] The lattice parameter change

Table I. The angle between the (220) and the selected crystalline plane

(*hkl*) plane	Angle (°)
(211)	30
(311)	31.48
(222)	35.26
(400)	45

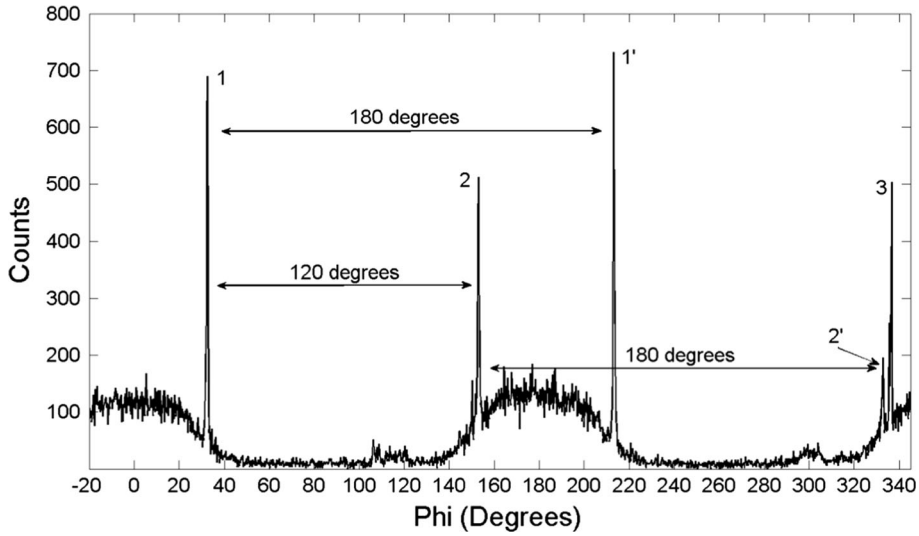

Fig. 8. An off-axis ϕ scan of the (211) LiZnAs. Peaks *1* and *1′* belong to one domain, and peaks *2* and *2́* belong to a second domain, and *3* belongs to a third domain.

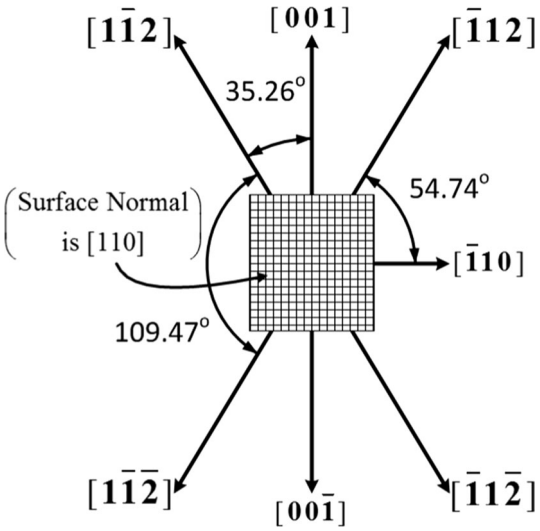

Fig. 9. A diagram of the angular relationship between the ⟨112⟩ LiZnAs directions on (110) LiZnAs.

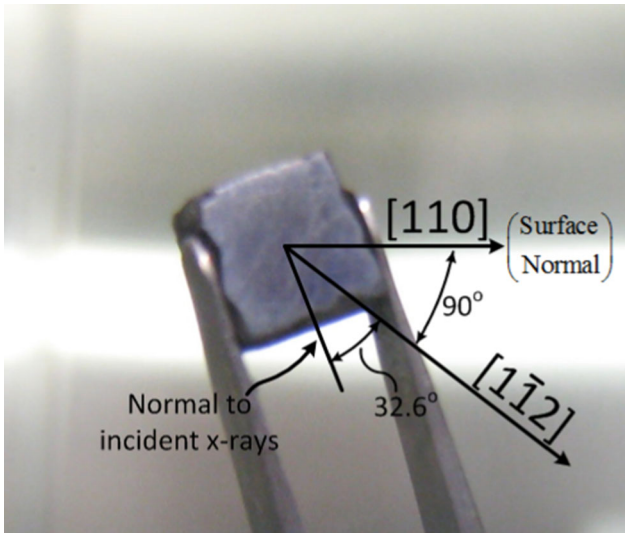

Fig. 10. The LiZnAs sample labeled with crystallographic relationships for the surface normal, and the first [1$\bar{1}$2] domain observed from the off-axis phi scan.

can be explained by considering semiconductor doping, or adding an excess of a particular element for compensation purposes for desired electrical properties.[33,34] The additives can alter the lattice parameters, therefore changing the lattice constant and *d*-spacing. In this study, the starting material was purified by a static sublimation process; however, an excess of an impurity yet remaining in material may be acting as a dopant, or a lack there of, due to the loss of lithium in this case, therefore, altering the lattice constant. Here, the lattice constant reduction was likely caused by the reduction of lithium atoms in the unit cell. For the desired application of neutron detectors, it may be necessary for device performance, or neutron sensitivity, that the bulk crystallization process be modified, where an excess of lithium is added to purified powders, where the lithium over-pressure may keep the volatile lithium from escaping. Encapsulation using a high-temperature material such as boron oxide may also be required to keep the right lithium balance for a lithium-rich F-43m LiZnAs unit cell.

The largest known crystalline ingots of LiZnAs were grown for the first time by a modified Bridgman high-temperature growth method. Crystal growth was carried out successfully using a crucible-lined tantalum vessel. The melting temperature observed was determined to be between 1230°C and 1250°C experimentally. A processed sample exhibited a (220) main orientation as characterized

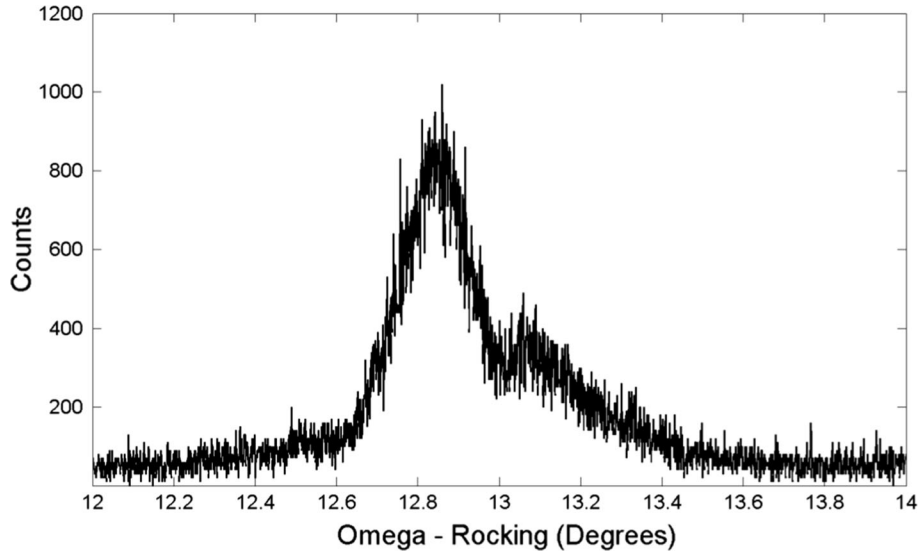

Fig. 11. An off-axis rocking curve of the (211) LiZnAs.

by EDXRD and high-resolution XRD. A reasonable degree of crystallinity and ordering was demonstrated from the out-of-plane and in-plane measurements. From the off-axis phi scans it was clear that three major domains were present in the characterized sample. Future work will include electrical characterization (resistivity, mobility-lifetime, trapping time), and neutron sensitivity measurements using these newly synthesized materials

ACKNOWLEDGEMENTS

Work was funded in part by the Advanced Materials program DOE–NNSA, Grant # DE-FEG52-08NA28766.

REFERENCES

1. B.W. Montag, M.A. Reichenberger, K.R. Arpin, M. Sunder, K.A. Nelson, P.B. Ugorowski, and D.S. McGregor, *J. Cryst. Growth* 412, 103 (2015).
2. B.W. Montag, M.A. Reichenberger, P.B. Ugorowski, M. Sunder, J. Weeks, and D.S. McGregor, *J. Cryst. Growth* 438, 99 (2016).
3. R. Juza, K. Langer, and K. Von Benda, *Angew. Chem. Int. Edit.* 7, 360 (1968).
4. H. Nowotny and K. Bachmayer, *Monatsh. Chem.* 81, 488 (1950).
5. D. Kieven, A. Grimm, A. Beleanu, C.G.F. Blum, J. Schmidt, T. Rissom, I. Lauermann, T. Gruhn, C. Felser, and R. Klenk, *Thin Solid Films* 519, 1866 (2011).
6. R. Bacewicz and T.F. Ciszek, *Appl. Phys. Lett.* 52, 1150 (1988).
7. K. Kuriyama, T. Katoh, and N. Mineo, *J. Cryst. Growth* 108, 37 (1991).
8. Z.W. Bell, K.R. Pohl, and L. Van Den Berg, *IEEE Trans. Nucl. Sci.* 51, 1163 (2004).
9. A.G. Vradii, M.I. Krapivin, L.V. Maslova, O.A. Matveev, A.K. Khusainov, and V.K. Shashurin, *At. Energy* 42, 64 (1977).
10. A.G. Beyerle and K.L. Hull, *Nucl. Inst. Methods A* 256, 377 (1987).
11. D.S. McGregor, J.T. Lindsay, and R.W. Olsen, *Nucl. Inst. Methods A* 381, 498 (1996).
12. Y. Kumashiro, K. Kudo, K. Matsumoto, Y. Okada, and T. Koshiro, *J. Less Common Met.* 143, 71 (1988).
13. W.C. McGinnis, *SPAWAR Systems Center*, Technical Report 19212003.
14. J.C. Lund, F. Olschner, F. Ahmed, and K. S. Shah, *MRS Online Proceedings Library*, vol. 162 (1989), p. 601.
15. F.P. Doty, *Boron Nitride Solid State Neutron Detector*, US-6727504 (2004).
16. A.N. Caruso, P.A. Dowben, S. Balkir, N. Schemm, K. Osberg, R.W. Fairchild, O.B. Flores, S. Balaz, A.D. Harken, B.W. Robertson, and J.I. Brand, *Mater. Sci. Eng. B* 135, 129 (2006).
17. B.W. Robertson, S. Adenwalla, A. Harken, P. Welsch, J.I. Brand, P.A. Dowben, and J.P. Claassen, *Appl. Phys. Lett.* 80, 3644 (2002).
18. P. Groot, J.H.F. Grondel, and P.J. Van Der Put, *Solid State Ion.* 16, 95 (1985).
19. A.N. Caruso, R.B. Billa, S. Balaz, J.I. Brand, and P.A. Dowben, *J. Phys. Condens. Matter* 16, L139 (2004).
20. D.S. McGregor, M.D. Hammig, Y.H. Yang, H.K. Gersch, and R.T. Klann, *Nucl. Inst. Methods A* 500, 272 (2003).
21. K. Kuriyama, T. Kato, and K. Kawada, *Phys. Rev. B Condens. Matter* 49, 11452 (1994).
22. K. Kuriyama and F. Nakamura, *Phys. Rev. B Condens. Matter* 36, 4439 (1987).
23. R. Bacewicz and T.F. Ciszek, *Acta Phys. Pol. A* A77, 379 (1990).
24. K. Kuriyama, T. Kato, T. Kato, and H. Matsuno, *J. Cryst. Growth* 166, 631 (1996).
25. W. Hoenle, *Z. Naturforsch. B Chem. Sci.* 48, 683 (1993).
26. S.H. Wei and A. Zunger, *Phys. Rev. Lett.* 56, 528 (1986).
27. B.W. Montag, M.A. Reichenberger, M. Sunder, P.B. Ugorowski, K.A. Nelson, and D.S. McGregor, *J. Cryst. Growth* 419, 143 (2015).
28. Bruker AXS Inc., "brochure_D2_CRYSO.pdf" (2014). http://bruker.poznan.pl/images/stories/AXS/brochure_D2_CRYSO.pdf. Accessed 3 April 2017.
29. R.E. Dinnebier and S.J.L. Billinge, *Powder Diffraction: Theory and Practice* (Cambridge: The Royal Society of Chemistry, 2008).
30. A. Le Bail, *Powder Diffr.* 20, 316 (2005).
31. W. Kraus and G. Nolze, *J. Appl. Cryst.* 29, 301 (1996).
32. J.P. Zhao, M.H. Quan, and L. Zhang, *Ceram. Int.* 32, 843 (2006).
33. W. Walukiewicz, L. Lagowski, L. Jastrzebski, M. Lichtensteiger, and H.C. Gatos, *J. Appl. Phys.* 50, 899 (1979).
34. F. Robert, *Pierret, Advanced Semiconductor Fundamentals*, 2nd ed. (Upper Saddle River: Pearson Education Inc, 2003).